INSTITUTE FOR FUSION STUDIES

DE-FG03-96ER-54346-743 IFSR #743

Study of Micro-instabilities in Toroidal Plasmas with Negative Magnetic Shear

J.Q. DONG,[a] Y.Z. ZHANG
International Center for Theoretical Physics
P.O. Box 586, 34100 Trieste, Italy
S.M. MAHAJAN
Institute for Fusion Studies, The University of Texas at Austin
Austin, Texas 78712 USA and
P.N. GUZDAR
Institute for Plasma Research, University of Maryland
College Park, MD 20742-3511

[a] *Present address: Southwestern Institute of Physics, Peoples Repub. of China*

March 1996

THE UNIVERSITY OF TEXAS

AUSTIN

Study of Micro-instabilities in Toroidal Plasmas with Negative Magnetic Shear

J.Q. Dong,[a] Y.Z. Zhang

International Center for Theoretical Physics

P.O. Box 586, 34100 Trieste, Italy

S.M. Mahajan

Institute for Fusion Studies, The University of Texas at Austin

Austin, Texas 78712 USA

and

P.N. Guzdar

Institute for Plasma Research, University of Maryland, College Park, MD 20742-3511

Abstract

The micro-instabilities driven by a parallel velocity shear, and a temperature gradient of ions are studied in toroidal plasmas with negative magnetic shear. Both the fluid and the gyro-kinetic formulations are investigated. It is found that for a broad range of parameters, the linear growth rates of the modes are lower, and the threshold temperature gradient η_{ic} is higher for plasmas with negative magnetic shear compared to plasmas with positive magnetic shear of equal magnitude. The reduction in the growth rate (with negative shear), although not insignificant, does not seem to be enough to account for the dramatic improvement in the confinement observed experimentally. Other possible physical mechanisms for the improved confinement are discussed.

[a]Permanent affiliation: Southwestern Institute of Physics, P.O. Box 432 Chengdu, People's Republic of China.

I. Introduction

Recent theoretical studies have shown, that the three key conditions for an economically attractive steady state tokamak fusion reactor, namely, high normalized beta, $\beta_N = \beta/(I/aB_0)$, stabilization of the most dangerous MHD and micro-instabilities, and a high fraction of self-sustained bootstrap current, may be achievable simultaneously in an optimized discharge scenario.[1,2] Here, $\beta \sim \langle p \rangle / B_0^2$ is the ratio of the plasma kinetic pressure to the magnetic field pressure, and is a measure of fusion reactivity and, therefore, of the efficiency of a fusion reactor. Also I is the total plasma current, a is the plasma minor radius, and B_0 is the toroidal magnetic field.

One of the crucial features of such a scenario is that there exists a region in the core of the plasma, where the magnetic shear is reversed ($dq/dr < 0$, with q being the safety factor, and r being the coordinate in the direction of the minor radius). A negative magnetic shear has several connected beneficial effects. It stabilizes the $n = \infty$ ideal MHD ballooning instability and therefore removes the constraint on the pressure gradient imposed by such modes. A high pressure gradient is necessary for a large ratio of the self-sustained bootstrap current to the total plasma current, which, in turn, helps to create a negative magnetic shear region close to the center of the plasma column. In addition, the negative magnetic shear is found to suppress the trapped electron mode,[3,4] which is believed to be one of the instabilities responsible for the anomalous transport in tokamaks

Recent experiments on the Joint European Torus (JET),[5] the Tokamak Fusion Test Reactor (TFTR),[6] and DIII-D[7] have demonstrated that particle and energy confinements are significantly improved resulting in higher ion density and temperature in a reversed magnetic shear region. Careful optimization of the discharge, through procedures such as pellet injection, neutral beam injection and current ramp-up, is needed to obtain the desired

plasma.

The ion temperature gradient (ITG or $\eta_i = d\ln T_i/d\ln n_i$) driven drift-like instability is currently the most plausible candidate for explaining the anomalous ion energy transport in tokamak plasmas. Numerous studies on this mode have been carried out theoretically and experimentally in the last decade. Most of these investigations, however, have been confined to plasmas with positive magnetic shear because negative magnetic shear plasmas are a comparatively new phenomenon.

In recent theoretical studies, it was reported[1] that the ITG mode is stabilized in a portion of the negative magnetic shear region for a proposed discharge with optimized plasma temperature, density and current profiles. However, the parametric dependence of the mode for a negative shear system is quite unknown and one needs to undertake a systematic investigation of the ITG mode in this new regime.

Motivated by the earlier experimental discovery[8,9] of a Parallel Velocity Shear (PVS) layer in the edge transport barrier region of tokamak plasmas (with the standard positive magnetic shear), momentum and energy transport from turbulence driven by PVS and ITG, have been studied for a sheared slab configuration.[8] On DIII-D tokamak,[7] high toroidal velocity shear is observed in the region where the confinement is improved with negative shear . The effects of negative magnetic shear on the instability driven by PVS is a new area of investigation. Although the mode characteristics are well understood and documented for a positive magnetic shear in a slab, not much is known for the negative shear case. It will be discussed in Sec. II that the sign of the magnetic shear does not affect the eigenvalue (either the real frequency or the growth rate) of the modes driven by PVS or ITG in a sheared slab. It is only in the toroidal configuration that the modes are sensitive to the sign of the magnetic shear.

In this work, the instabilities driven by PVS and ITG are first studied using a fluid

theory in a toroidal plasmas with both positive and negative magnetic shear. The results are valid for long wavelength perturbations in relatively low temperature plasmas. For short wavelength perturbations in high temperature plasmas, the gyrokinetic theory, which takes into account the full parallel transit and the finite ion Larmor radius effects, has to be applied. In recent years,[10-12] several such codes have been developed and documented for the linear instability studies. In this work, the integral dispersion equation for low frequency toroidal drift-like modes, derived and given in detail in Ref. 12, is applied to study the effects of the negative magnetic shear on the kinetic ITG mode. The parametric dependence of the instability is investigated systematically. Particular attention is given to those features of the mode which depend solely on the sign of the magnetic shear.

The contents of this work are organized as follows. In Sec. II a general theory for the slab modes, with arbitrary sign for the magnetic shear, is presented. This part of the work shows the necessity for adopting a toroidal geometry to reflect the differences between systems with positive and negative shear. In Sec. III, the fluid dispersion equation in the toroidal geometry for the study of PVS and ITG driven instabilities is derived, and numerically solved. The results from the integral dispersion equation are presented in Sec. IV, and Sec. V is devoted to conclusions and discussion.

II. Fluid theory in slab geometry

The magnetic shear, defined as $\hat{s} = rdq/qdr$ (q is the safety factor, and r is the radial coordinate), is a measure of the relative radial change of the pitch of a magnetic field line. For a slab configuration, the magnetic field takes the form $\mathbf{B} = B_0[\hat{\mathbf{z}} + (x/L_s)\hat{\mathbf{y}}]$, with $L_s = Rq/\hat{s}$ displaying the reflection symmetry about the mode rational surface $x = 0$. This feature has important consequences as shown through a proper analysis of the linear eigenmode equation governing the behavior of the instabilities driven by PVS and ITG in a

slab geometry. The normalized equations for these modes[8] are

$$\frac{d^2\phi(x)}{dx^2} - b_s\phi(x) + \frac{1-\widehat{\omega}}{\widehat{\omega}+K}\phi(x) + \left[\frac{\widehat{s}^2x^2}{\widehat{\omega}^2} - \frac{\widehat{v}'_{0\|}\widehat{s}x}{(\widehat{\omega}+K)\widehat{\omega}}\right]\phi(x) = 0, \tag{1}$$

where

$$b_s = k_y^2\rho_s^2, \quad K = \frac{(\eta_i+1)}{\tau},$$
$$\widehat{\omega} = \frac{\omega}{\omega_{*e}}, \quad \tau = \frac{T_e}{T_i}, \quad \widehat{v}'_{0\|} = \frac{L_n dv_{0\|}}{c_s dx},$$

and ω_{*e} is the electron diamagnetic drift frequency. The variable x in Eq. (1) is normalized to $\rho_s = c_s/\Omega$ with c_s being the sound speed and Ω being the ion gyrofrequency. The magnetic shear $\widehat{s}$, has also been redefined for the slab case as L_n/L_s. Both $\widehat{s}$ and the variable x appear as squared quantities in Eq. (1) when $\widehat{v}'_{0\|} = 0$. As a result, the eigenvalue $\widehat{\omega}$ is independent of the sign of $\widehat{s}$, and the eigenfunction $\phi(x)$ is symmetric in this case. It is apparent, that the solution may depend on the sign of the magnetic shear $\widehat{s}$ when $\widehat{v}'_{0\|} \neq 0$. It does affect the eigenfunction, but not the eigenvalue. This can be readily seen by examining the solution of equation (1). The eigenvalue condition obtained from Eq. (1) is

$$-b_s - \frac{1-\widehat{\omega}}{\widehat{\omega}+K} - \frac{\widehat{v}'^2_{0\|}}{4(\widehat{\omega}+K)^2} = i|\widehat{s}|(2n+1). \tag{2}$$

The corresponding eigenfunction is

$$\phi^{(n)}(x) = \phi_0^{(n)} H_n\left[\sqrt{\frac{i|\widehat{s}|}{\widehat{\omega}}}(x+\Delta)\right] \exp\left[\frac{i|\widehat{s}|(x+\Delta)^2}{2\widehat{\omega}}\right], \tag{3}$$

where H_n is the Hermite function of order n and

$$\Delta = -\frac{\widehat{v}'_{0\|}\widehat{\omega}}{2\widehat{s}(\widehat{\omega}+K)}. \tag{4}$$

Only the $n = 0$ mode will be discussed hereafter. Equation (2) clearly reveals that the eigenvalue is independent of the signs of both the magnetic as well as the velocity shear. However, the sign of $\widehat{s}$ does affect the eigenfunction $\phi(x)$ as is indicated in Eqs. (3) and (4). The asymmetry introduced by a finite Δ, a shift of the position of the maximum $\phi^{(0)}(x)$

from the mode rational surface ($x = 0$), depends on the sign of $\hat{s}$. Δ is a real shift in x space in the cold ion approximation ($K \to 0$). In general, Δ is complex and induces a deformation in addition to a mere translation.

It is clear from the previous discussion that the mode frequency in the slab geometry depends only on the magnitude of the shear parameter and is insensitive to its sign. Let us now reconsider the fluid theory of PVS and ITG modes in toroidal geometry to investigate the possible effects of the negative magnetic shear. A similar study for the kinetic equation (Ref. 13) will also be undertaken.

The major relevant effects introduced by the toroidicity of the magnetic configuration are contained in the drifts induced by the gradient, and the curvature of the magnetic field. These are proportional to

$$\omega_D^* = (\cos k + \hat{s} k \sin k), \tag{5}$$

where the first and the second terms come from the principal, and the geodesic curvatures, respectively, and k is the extended poloidal angle of the well-known ballooning representation. The function $\omega_D^*(k)$ is plotted in Fig. 1 for five different values of $\hat{s}$. It is clearly shown that the sign of the magnetic shear $\hat{s}$ introduces a dramatic change in the toroidal drifts. The change comes mainly from the geodesic curvature drift. The biggest effect is expected to take place for the modes localized around $k \sim 2$ where the dependence of the drift frequency ω_D^* on the magnetic shear is the strongest. A clear physical picture of the effect of negative shear on curvature driven modes has recently been presented in Ref. 14.

III. Fluid theory in toroidal geometry

The eigenmode equation for the PVS and ITG driven fluid instabilities in toroidal plasmas is,

$$\left\{ A\frac{d^2}{dk^2} + B\frac{d}{dk} + C \right\} \phi(k) = 0, \tag{6}$$

where

$$A = \frac{\widehat{\omega} + K}{\widehat{\omega}}, \tag{7}$$

$$B = \frac{i\widehat{v}'_{0\parallel} q \widehat{k}_\theta}{\epsilon_n}, \tag{8}$$

$$C = \left(\frac{q\widehat{k}_\theta}{\epsilon_n}\right)^2 \left[\widehat{\omega}(\widehat{\omega}-1) + (\widehat{k}_\theta \widehat{s})^2 \widehat{\omega}(\widehat{\omega}+K)\left(k^2 + \frac{1}{\widehat{s}^2}\right) + \alpha 2\epsilon_n \omega_D^*(\widehat{\omega}+K)\right], \tag{9}$$

ω_D^* is given in Eq. (5), $\epsilon_n = L_n/R$, R is the major radius, and $\widehat{k}_\theta$ is normalized to ρ_s^{-1}. A factor α has been put in the front of the last term in Eq. (9) to explicitly identify the toroidicity effects; $\alpha = 0$ corresponds to the slab, and $\alpha = 1$ to the toroidal case. It is worth pointing out that the toroidal term is proportional to ϵ_n as it should be. It is also clear that Eq. (6) is the Fourier transform of the x space equation (1) which is used to study the same instabilities in a slab,[8] i.e. when $\alpha = 0$.

Introducing

$$\phi(k) = \overline{\phi}(k) e^{\sigma k}, \tag{10}$$

with

$$\sigma = -\frac{B}{2A} = \frac{-i\widehat{\omega} q \widehat{k}_\theta \widehat{v}'_{0\parallel}}{2(\widehat{\omega}+K)\epsilon_n}, \tag{11}$$

Eq. (6) becomes

$$\left[\frac{d^2}{dk^2} + \left(\frac{\widehat{\omega} q \widehat{k}_\theta}{\epsilon_n}\right)^2 Q(\widehat{\omega}, k)\right] \overline{\phi}(k) = 0, \tag{12}$$

where

$$Q(\widehat{\omega}, k) = \frac{\widehat{v}'^2_{0\parallel}}{4(\widehat{\omega}+k)^2} + \frac{\widehat{\omega}-1}{\widehat{\omega}+K} + \widehat{k}_\theta^2(1+\widehat{s}^2 k^2) + \alpha \frac{2\epsilon_n}{\widehat{\omega}} \omega_D^*. \tag{13}$$

Again Eq. (12) reduces to the equation studied numerically and analytically in Ref. 15 when the velocity shear and the ion temperature are taken to be zero, i.e. $\widehat{v}'_{0\parallel} = K = 0$.

Taking the PVS and the ITG effects into account, Eq. (12) is solved numerically with a shooting code. The results are presented in the next four subsections.

A. Cold ion limit

In Fig. 2(3), the normalized growth rate and the real frequency of the mode, driven by a PVS ($\widehat{v}'_{0\parallel}$) in the cold ion limit ($T_i \ll T_e$) are plotted as function of the magnetic shear for $\widehat{s} > 0$ ($\widehat{s} < 0$). The other plasma parameters are $\widehat{k}_\theta^2 = 0.1$, $\widehat{v}'_{0\parallel} = 1$, and $\epsilon_n = 0.2$. Figures 2(a) and 3(a) show that for a given $|\widehat{s}|$ the growth rate scaling with the magnetic shear is different for $\widehat{s} < 0$ and $\widehat{s} > 0$. The growth rate decreases monotonically with decreasing $\widehat{s}$ for $\widehat{s} < 0$ while for $\widehat{s} > 0$, it first increases in the range $0 \leq \widehat{s} \leq 1$, and then decreases for $\widehat{s} \geq 1$. Generally speaking, the stabilizing effect of the magnetic shear is always stronger for the negative sign, $\widehat{s} < 0$, for the plasmas studied here. However, it is only in the intermediate range $0.5 < |\widehat{s}| < 1$ that the differences can be substantial. For high ($|\widehat{s}| \sim 2$) as well as low ($|\widehat{s}| \sim 0.1$) shear, the growth rates tend to be close. For example, when $q = 1.5$, the growth rate for $\widehat{s} = 0.1$ is $\gamma/\omega_{*e} = 0.265$ and for $\widehat{s} = -0.1$, the growth rate is $\gamma/\omega_{*e} = 0.237$. For $|\widehat{s}| = 1$, however, the growth rates are respectively 0.36 and 0.09 for the positive and the negative shear. Another clear message of Figs. 2(a) and 3(a) is that the stabilization brought about by negative magnetic shear is stronger for lower q plasmas. For $q \geq 4.5$, the dependence of the growth rates on magnetic shear is very weak. The real frequency, on the other hand, increases slowly with the decrease in $|\widehat{s}|$ for $\widehat{s} < 0$, while it decreases almost linearly with $\widehat{s}$ up to $\widehat{s} \sim 0.75$ and becomes independent of shear for $\widehat{s} > 1$ (Figs. 2(b) and 3(b)).

B. Finite ion temperature and ITG effects

The finite ion temperature ($T_i = T_e$) and ITG ($\eta_i = 1,\ 4$) effects are considered in this subsection. The mode growth rate, and the real frequency are plotted in Fig. 4 for $\widehat{s} = 1$ and -1 with $q = 3$, $\widehat{v}'_{0\parallel} = 1$ when the toroidicity parameter ϵ_n varies from 0.05 to 0.6. Again, the mode is less unstable for $\widehat{s} < 0$ than it is for $\widehat{s} > 0$. The difference in the growth rates (for fixed

plasma parameters) for equal magnitude positive and negative magnetic shear increases with the toroidicity parameter ϵ_n. For example, the growth rates ($\eta_i = 4$) are $\gamma/\omega_{*e} = 0.73$ and 0.59 for $\hat{s} = 1$ and -1 for $\epsilon_n = 0.05$, and they respectively rise to 2.4 and 1.8 for $\epsilon_n = 0.6$: all other parameters remain unchanged. The real frequencies increase approximately linearly with ϵ_n, and hardly change when the magnetic shear is reversed (Fig. 4(b)). The mode propagates in the electron diamagnetic drift direction in a cold ion plasma. The direction of propagation changes to the ion drift direction when finite ion temperature and finite ITG effects are included and ϵ_n is not too small. The direction of propagation is also a strong function of η_i.

C. Toroidicity drive

The strength of the toroidal term in Eq. (6) is proportional to α; α=0 implies no toroidal effects while α=1 corresponds to the full inclusion of toroidal drifts. In Fig. 5, we plot the mode growth rate, and real frequency as a function of α for both $\hat{s} = -1,\ 1$, and $\epsilon_n = 0.2,\ 0.4$ when the others parameters are $\hat{k}_\theta^2 = 0.1,\ \eta_i = 5,\ \hat{v}'_{0\parallel} = 0,\ \tau = 1,\ q = 2$. We had seen in Sec. II, that sign of $\hat{s}$ becomes relevant only when the toroidicity is taken into account; the eigenvalues are the same for $\hat{s} = -1$ and $\hat{s} = 1$ when $\alpha = 0$ (for a slab). The difference between the growth rates for the opposite signs of the shear for the same $|\hat{s}|$ increase approximately linearly with the toroidicity factor α, and reaches a maximum at $\alpha = 1$. The real frequency behaviour is a bit more complicated. The frequency in a torus is lower than it is in a slab for $\hat{s} = 1$, while it is higher than the slab value for $\hat{s} = -1$, for $\epsilon_n = 0.4$. For a different $\epsilon_n = 0.2$, the real frequency changes little for $\hat{s} = -1$ as α increases from zero to one. However for $\hat{s} = 1$, the real frequency decreases to one half its value as we sweep α from zero to one.

It is important to point out that the entire previous discussion pertains to the slab-like branch and not to the toroidicity induced one. The mode studied here has a well-defined slab

limit. In addition, from the previous discussion, we have all the reasons to predict that the sign of the magnetic shear may have a very strong effect on the toroidicity induced branch.

D. Structure of eigenfunction

The typical eigenmode structures in the ballooning space $\bar{\phi}(k)$ are shown in Fig. 6 for $\hat{k}_\theta^2 = 0.1$, $\hat{v}'_{0\|} = 0$, $\eta_i = 7$, $\tau = 1$, $\epsilon_n = 0.2$, $q = 3$, and $\hat{s} = -1,\ 1$. The widths of the real part of the wavefunctions are very similar for the two cases, while the imaginary part for $\hat{s} = 1$ is approximately twice as wide as the imaginary part for $\hat{s} = -1$. The eigenmodes are trapped in the region of $-1.5 < k < 1.5$ where the difference between the toroidicity drifts for $\hat{s} = -1$ and 1 is not significant (see Fig. 1).

IV. Gyrokinetic analysis

In the fluid theory presented in the last section, the kinetic effects such as Landau damping and finite Larmor radius of the ions were neglected. In this section, the integral gyrokinetic eigenmode equation, which includes the full ion dynamics, except the bounce motion due to toroidicity, is used to investigate the kinetic ITG mode in a toroidal plasma with negative magnetic shear. The equation has been derived and described in detail in earlier work[12,16] and will not be repeated here. We shall now numerically solve Eq.(12) of Ref. 12 for negative shear, $\hat{s} < 0$, systems and compare the results with the standard positive shear, $\hat{s} > 0$, case.

A. Magnetic shear variation

Here we compare growth rates for $\hat{s} > 0$ and $\hat{s} < 0$ while other plasma parameters are kept unchanged. The normalized growth rate of the kinetic ITG mode in toroidal plasmas is plotted, in Fig. 7, as a function of $\hat{s}$ for $\eta_i = 2.5$, $T_e/T_i = 1$, $k_\theta \rho_i = 0.5$, $\epsilon_n = 0.25$, $q =$ 1.5, 2.0, 2.5, and 3. As in the fluid case, the growth rate decreases monotonically with

increasing $|\hat{s}|$ for negative magnetic shear (Fig. 7(a)). For $\hat{s} > 0$ (Fig. 7(b)), the growth rate first increases, reaches a maximum at $\hat{s} \sim 0.5$, and then decreases with increasing $\hat{s}$. The maximum growth rate for $q = 3$, and $\hat{s} = 0.5$, $\gamma/\omega_{*e} \sim 0.48$ is just a bit greater than the growth rate $\gamma/\omega_{*e} \sim 0.4$ for $q = 3$, $\hat{s} = -0.5$ Similar to what was found in the fluid theory for the PVS mode in cold plasmas, the stabilizing effects of the negative magnetic shear are strongest for lower q plasmas. For example, for $q = 1.5$, $\gamma/\omega_{*e} \sim 0.4$, at $\hat{s} = 0.5$ while $\gamma/\omega_{*e} \sim 0.2$ for $\hat{s} = -0.5$. On the other hand, the growth rates for $q = 3$ and $|\hat{s}| = 0.5$ are respectively 0.46 and 0.36 for the positive and the negative shear. Thus it seems that the negative shear has a significant stabilizing effect only for rather low q plasmas.

B. η_i variation

The normalized ITG eigenvalues, as a function of the parameter η_i, are presented in Fig. 8, where the open symbols are for $k_\theta \rho_i = 0.5$, the closed ones are for $k_\theta \rho_i = 0.75$; the circles are for $|\hat{s}| = 0.5$, the squares are for $|\hat{s}| = 1$, and the triangles are for $|\hat{s}| = 1.5$. The other parameters are $T_e/T_i = 1$, $\epsilon_n = 0.2$, $q = 2$; $\hat{s} < 0$ in Figs. 8(a) and 8(c), and $\hat{s} > 0$ in Fig. 8(b). The comparison of Fig. 8(a) and Fig. 8(b) shows that the mode growth rate is always lower for $\hat{s} < 0$ than that for $\hat{s} > 0$ for otherwise identical plasmas (including the magnitude of $\hat{s}$). In addition, we find that the lowest threshold values are: $\eta_{icr} \sim 0.9$ for $\hat{s} = 0.5$, $k_\theta \rho_i = 0.5$, and $\eta_{icr} \sim 1.2$ for $\hat{s} = -0.5$, $k_\theta \rho_i = 0.75$. For η_i close to η_{icr}, the normalized growth rate for the fastest growing modes may be approximated as

$$\frac{\gamma}{\omega_{*e}} = \kappa(\eta_i - \eta_{icr}) \tag{14}$$

where $\kappa = 0.2$ for $\hat{s} < 0$, and $\kappa = 0.3$ for $\hat{s} > 0$; the η_{icr}'s are given above. The highest η_{icr} values found here are 1.6 for $\hat{s} = -1.5$, and 1.7 for $\hat{s} = 1.5$, respectively. However, even for those parameters ($|\hat{s}| = 1.5$, $k_\theta \rho_i = 0.75$) the growth rate increases faster in the positive shear case than it does in the negative shear case when η_i increases. The graph of

real frequency versus η_i for $\hat{s} < 0$ is given in Fig. 8(c). Similar results, for $\hat{s} > 0$, are readily available in literatures.[12] Generally speaking, for a given plasma, the real frequency for $\hat{s} < 0$ is a factor of 1.5-2 lower than that for $\hat{s} > 0$.

C. $k_\theta \rho_i$ spectrum

We begin with a case of low toroidicity, $\epsilon_n = 0.2$. For this case, the mode growth rate, and the real frequency normalized to $\omega_{*e}/k_\theta \rho_i$ are plotted , in Fig. 9, as functions of $k_\theta \rho_i$. The open symbols are for $\hat{s} = 1$, the closed ones are for $\hat{s} = -1$; the circles are for $\eta_i = 3$ while the squares are for $\eta_i = 2$; other relevant parameters are $q = 2$, $T_e/T_i = 1$. It is clear from Fig. 9(a) that the difference between the growth rates for positive and negative magnetic shears are large for long wavelength perturbations ($k_\theta \rho_s \sim 0.3$) and small for short wavelength perturbations $k_\theta \rho_s \geq 1$. Again, the real frequencies of the mode (Fig. 9(b)) are lower for $\hat{s} < 0$ than that for $\hat{s} > 0$ if plasmas with the same $|\hat{s}|$ and other parameters are compared. It is evident from Fig. 9 that there is no significant difference between either the eigenvalues or the unstable $k_\theta \rho_i$ range for positive and negative magnetic shears in this parameter regime.

We have already learnt that the sign of the magnetic shear becomes significant when the toroidicity parameter ϵ_n increases. We illustrate this situation by increasing the toroidicity for the graphs of Fig. 10 where we plot the normalized growth rates $\gamma k_\theta \rho_i/\omega_{*e}$ versus the normalized poloidal wave vector $k_\theta \rho_i$ for $\epsilon_n = 0.3$, and 0.45. The open symbols are for $\hat{s} = 0.5$ while the closed ones are for $\hat{s} = -0.5$; the squares are for $\epsilon_n = 0.45$ and the circles are for $\epsilon_n = 0.3$. The other parameters are $\eta_i = 2.5$, $q = 1.5$, $T_e/T_i = 1$. For the same plasma conditions, the maximum growth rate for $\hat{s} < 0$ is less than one half of that for $\hat{s} > 0$. Furthermore, the unstable $k_\theta \rho_s$ region for negative shear is considerably smaller than that for a positive shear when $\epsilon_n = 0.45$. A combination of toroidicity with kinetics does bring out the fact that the negative shear plasmas are more stable to the well-known ITG mode.

V. Conclusions and discussion

The micro-instabilities driven by PVS and ITG are investigated using both the fluid, and the gyrokinetic theories. The correct fluid eigenmode equation, Eq. (6), which has both the PVS and ITG modes, is derived for toroidal plasmas. This equation is solved numerically for a wide range of plasma parameters for both positive and negative magnetic shear. It is found that for a given plasma (including the shear magnitude), the growth rates of both the PVS and ITG modes, are lower for $\hat{s} < 0$ than that for $\hat{s} > 0$. The differences occurs because the toroidal terms in the mode equation are sensitive to the sign of the magnetic shear.

A numerical solution of the integral gyrokinetic dispersion equation (with toroidicity) for the ITG mode shows not only lower growth rates but also higher values for critical η_i for the negatively sheared plasmas. Toroidal plasmas with negative shear are found to be definitely more stable than the standard positive shear plasmas.

The stronger stabilization effect of a negative magnetic shear, compared with a positive shear in both the fluid and gyrokinetic theories, mainly comes from the geodesic curvature drift, which changes direction when the magnetic shear changes sign. The differences between the mode growth rates for positive and negative magnetic shears increase significantly when the toroidicity parameter ϵ_n increases or the safety factor q decreases.

There is now experimental evidence that particle and ion energy confinements are significantly improved, and higher ion density and temperature are achieved in a reversed magnetic shear region.[5–7] The results reported in this paper are in qualitative agreement with these experimental observations. The lower growth rates and higher threshold values for PVS and ITG driven instabilities in plasmas with negative magnetic shear, $\hat{s} < 0$, may play some role in improving confinement in the regions of reversed magnetic shear. But a serious caveat is in order, here. Our theoretical estimates show that the differences between the strengths of the instabilities for positive and negative magnetic shears are perhaps not sufficient to account

for the experimentally observed dramatic improvement in confinement. In all likelihood, other more effective mechanisms have to be invoked to understand such severe reduction in transport.[5-7]

We must also remember that there is a finite transition region where the magnetic shear is close to zero. Most of the existing theories are not valid for this important and interesting region. Brand new mode equations, valid in the zero shear region , will be needed to develop a believable micro-instability theory. It is only then that a definite verdict on the connection between improved confinement and the mode stabilization in the new shear regime can be given. Experiment show that the best confinement region is in the neighborhood of zero shear.[5,7] We speculate that zero magnetic shear region contributes essentially to the experimentally observed confinement improvement. Detailed investigation is in progress and the results will be published later.

It may be pertinent, here, to note that, in a region of low magnetic shear, the perpendicular velocity shear v'_E induces a dramatic stabilization of the ITG and PVS modes.[13] This effect becomes even more interesting when one notices that PVS enhances the ITG instability in plasmas (with or without finite v'_E) with intermediate to high magnetic shear; while it has a stabilization effect on the ITG modes when the magnetic shear is low and v'_E is non-zero. All these observations definitely indicate that a serious investigation of the low shear regime is strongly warranted in order to understand the 'improved confinement' experiments.

Acknowledgments

Two of the authors (JQD and YZZ) would like to thank the staff at the International Center for Theoretical Physics, Trieste, Italy for their hospitality.

This work was supported in part by the U.S. Dept. of Energy contract No. DE-FG03-96ER-54346.

References

1. C. Kessel, J. Manickam, G. Rewoldt, and W.M. Tang, Phys. Rev. Lett. **72**, 1212 (1994).

2. A.D. Turnbull, T.S. Taylor, Y.R. Lin-Liu, and H. St. John, Phys. Rev. Lett. **74**, 718 (1995).

3. B.B. Kadomtsev and O.P. Pogutse, Zh. Eksp. Teor. Fiz. **51**, 1734 (1966) [Sov. Phys. JETP **24**, 1172 (1967)].

4. M.N. Rosenbluth and M.L. Sloan, Phys. Fluids **14**, 1725 (1971).

5. M. Hugon, B.Ph. van Milligen, P. Smeulders, L.C. Appel, D.V. Bartlett, D. Doucher, A.W. Edwards, L.-G. Eriksson, C.W. Gowers, T.C. Hender, G. Huysmans, J.J. Jacquinot, P. Kupschus, L. Porte, P.H. Rebut, D.F.H. Start, F. Tibone, B.J.D. Tubbing, M.L. Watkins, and W. Zwingmann, Nucl. Fusion **32**, 33 (1992).

6. F.M. Levinton, M.C. Zarnstorff, S.H. Batha, M. Bell, R.V. Budny, C. Bush, Z. Chang, E. Fredrickson, A. Janos, J. Manickam, A. Ramsey, S.A. Sabbagh, G.L. Schmidt, E.J. Synakowski, and G. Taylor, Phys. Rev. Lett. **75**, 4417 (1995).

7. E.J. Strait, L.L. Lao, M.E. Mauel, B.W. Rice, T.S. Taylor, K.H. Burrell, M.S. Chu, E.A. Lazarus, T.H. Osborne, S.J. Thompson, and A.D. Turnbull, Phys. Rev. Lett. **75**, 4421 (1995).

8. J.Q. Dong, W. Horton, R. Bengtson, G.X. Li, Phys. Plasmas **1**, 3250 (1994).

9. Y. Koide, M. Kikuchi, S. Ishida, M. Mori, S. Tsuji, N. Asakura, Y. Kmada, T. Nishitani, Y. Kawano, T. Hatae, T. Fujita, T. Fukuda, N. Asakura, T. Kondoh, R. Yoshino, and Y. Neyatani, Phys. Rev. Lett. **72**, 3662 (1994).

10. G. Rewoldt and W.M. Tang, Phys. Fluids B **2**, 318 (1990).

11. F. Romanelli, Phys. Fluids B **1**, 1018 (1989).

12. J.Q. Dong, W. Horton, J.-Y. Kim, Phys. Fluids B **4**, 1867 (1992).

13. J.Q. Dong and W. Horton, Phys. Fluids B **5**, 1581 (1993).

14. T. Antonsen Jr., J.F. Drake, P.N. Guzdar, A.B. Hassam, T.-T. Lau, and S.V. Novakovski, "Physical mechanism for the stabilization of Ballooning modes due to negative shear" to appear in Phys. Plasmas Lett.

15. Liu Chen and C.Z. Cheng, Phys. Fluids **23**, 2242 (1980).

16. J.Q. Dong and W. Horton, Phys. Plasmas **2**, 3412 (1995).

Figure Captions

1. Toroidal drift frequency as function of the extended poloidal angle k for $\hat{s} = -1, \ , -0.5, \ 0, \ 0.5,$ and 1.

2. (a) Mode growth rate and (b) real frequency versus magnetic shear $\hat{s} > 0$ for q=1.5, 2, 3, and 4.5 from the fluid theory with cold ions. The other parameters are $b_s = 0.1, \ \hat{v}'_{0\|} = 1, \ \epsilon_n = 0.2.$

3. The same as Fig. 2 but for $\hat{s} < 0$.

4. (a) Mode growth rate and (b) real frequency versus ϵ_n for $\hat{s} = -1, \ 1$ and $\eta_i = 1, \ 4$ from the fluid theory. The other parameters are $b_s = 0.1, \ q = 3, \ \hat{v}'_{0\|} = 1,$ and $T_e/T_i = 1.$

5. (a) Mode growth rate and (b) real frequency as functions of toroidicity factor α for $\hat{s} = -1, \ 1,$ and $\epsilon_n = 0.2, \ 0.4.$ the other parameters are $b_s = 0.1, \ \eta_i = 5, \ \hat{v}'_{0\|} = 0, \ q = 2,$ and $T_e/T_i = 1.$

6. The eigenmode structure in k space for $\hat{s} = -1, \ 1, \ b_s = 0.1, \ \eta_i = 7, \ T_e/T_i = 1, \ \epsilon_n = 0.2, \ q = 3. \ \hat{v}_{0\|} = 0.$ The curves reaching the maxima 1 at $k = 0$ are the real parts while the curves having maxima 0.7 are the imaginary parts.

7. Mode growth rate as function of magnetic shear $\hat{s}$ for (a) $\hat{s} < 0$ and (b) $\hat{s} > 0$. The other parameters are $\eta_i = 2.5, \ T_e/T_i = 1, \ \epsilon_n = 0.25, \ k_\theta \rho_s = 0.5,$ and $q = 1.5, 2, 2.5$ and 3.

8. The growth rate for (a) $\hat{s} < 0$ and (b) $\hat{s} > 0$, and (c) the real frequency for $\hat{s} < 0$ versus η_i. The other parameters are $T_e/T_i = 1, \ \epsilon_n = 0.2, \ q = 2, \ k_\theta \rho_i = 0.5,$ and 0.75.

9. (a) The normalized growth rate and (b) the real frequency versus $k_\theta \rho_i$ for $\hat{s} = -1, \ 1.$ The other parameters are $T_e/T_i = 1, \ q = 2, \ \epsilon_n = 0.2, \ \eta_i = 2,$ and 3.

10. The normalized growth rate versus $k_\theta \rho_i$ for $\hat{s} = -0.5,\ 0.5$. The other parameters are $\eta_i = 2.5,\ T_e/T_i = 1,\ q = 1.5,\ \epsilon_n = 0.3$, and 0.45.

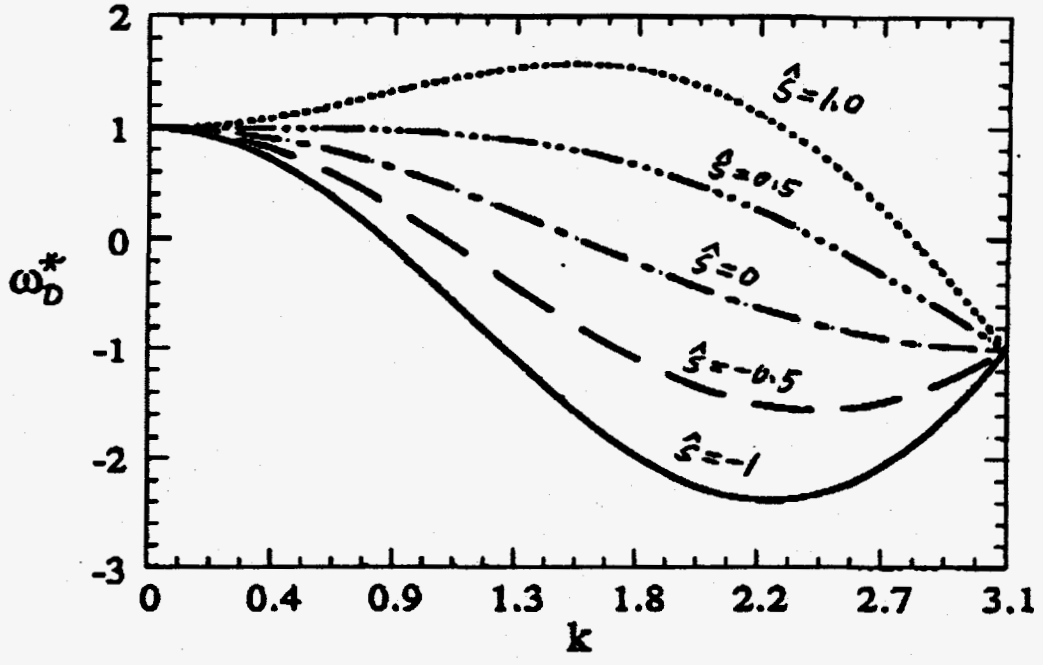
2
1
0
-1
-2
-3
ω_D^*
$\hat{s}=1.0$
$\hat{s}=0.5$
$\hat{s}=0$
$\hat{s}=-0.5$
$\hat{s}=-1$
0
0.4
0.9
1.3
1.8
2.2
2.7
3.1
k

Fig.1

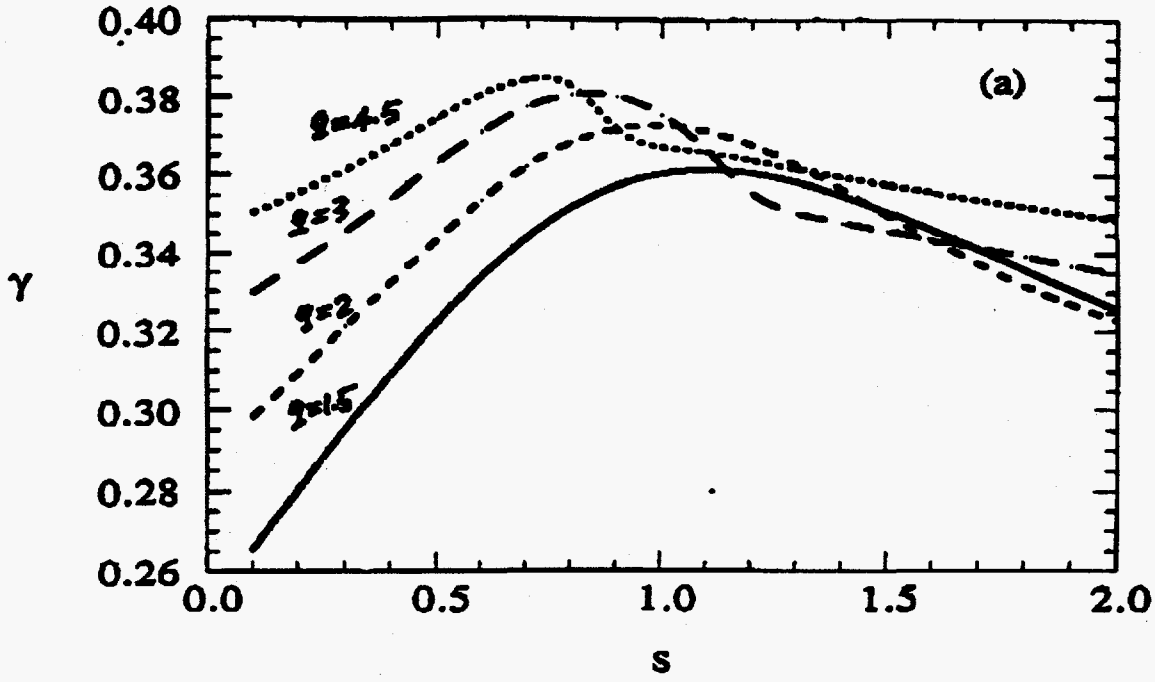
(a)
γ
0.40
0.38
0.36
0.34
0.32
0.30
0.28
0.26
0.0
0.5
1.0
1.5
2.0
s
q=4.5
q=3
q=2
q=1.5

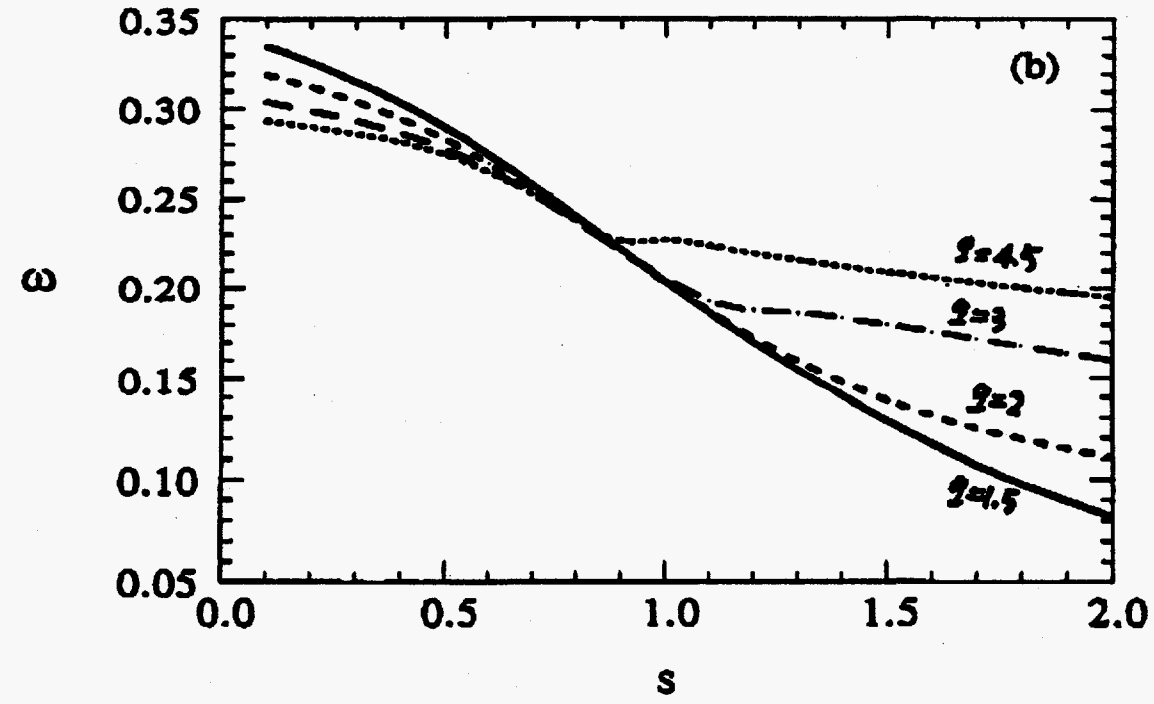
(b)
ω
0.35
0.30
0.25
0.20
0.15
0.10
0.05
0.0
0.5
1.0
1.5
2.0
s
q=4.5
q=3
q=2
q=1.5

Fig.2

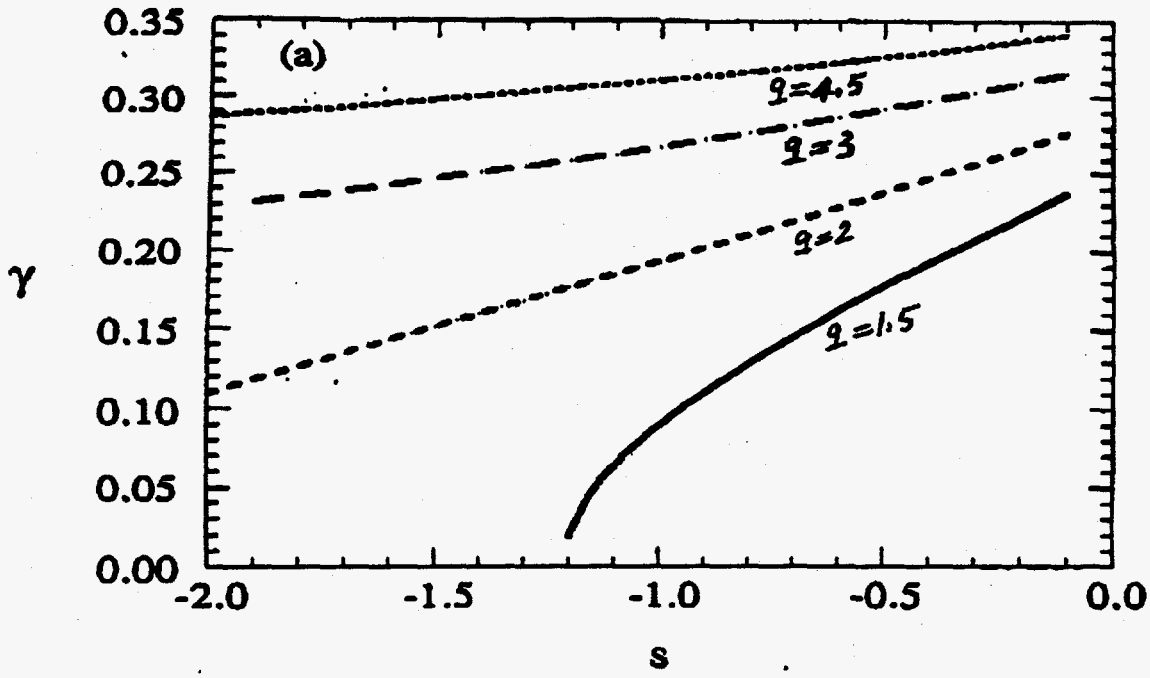
(a)
q=4.5
q=3
q=2
q=1.5
γ
0.35
0.30
0.25
0.20
0.15
0.10
0.05
0.00
-2.0
-1.5
-1.0
-0.5
0.0
s

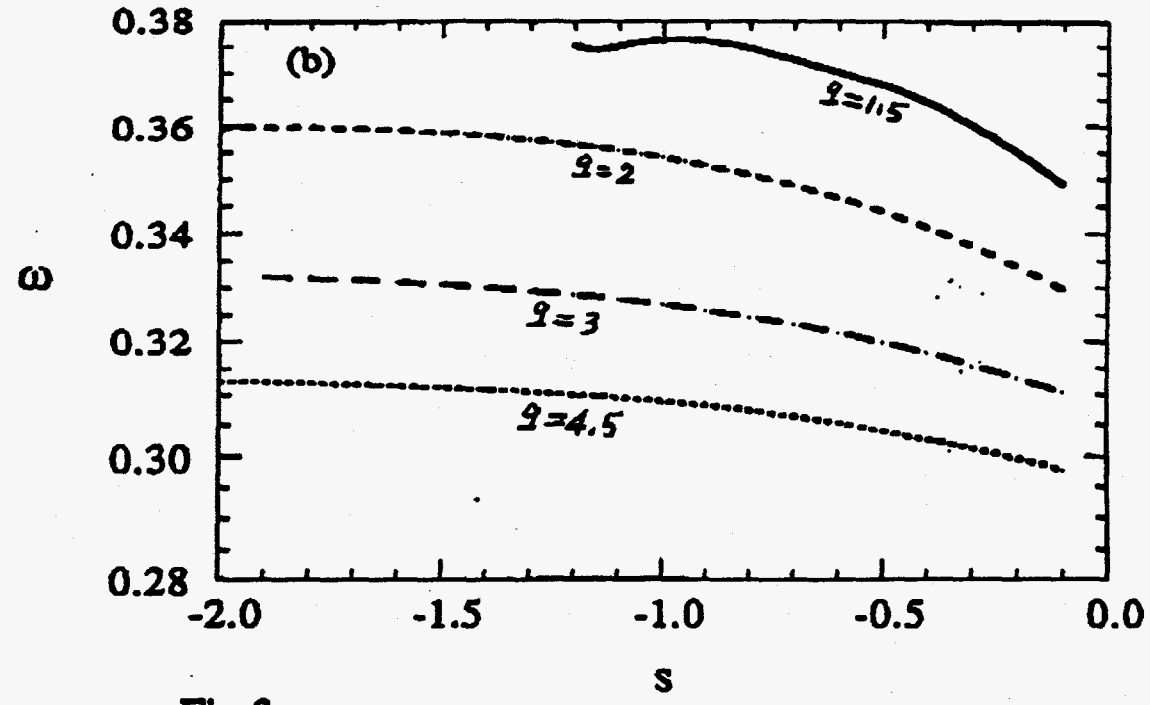
(b)
q=1.5
q=2
q=3
q=4.5
ω
0.38
0.36
0.34
0.32
0.30
0.28
-2.0
-1.5
-1.0
-0.5
0.0
s

Fig.3

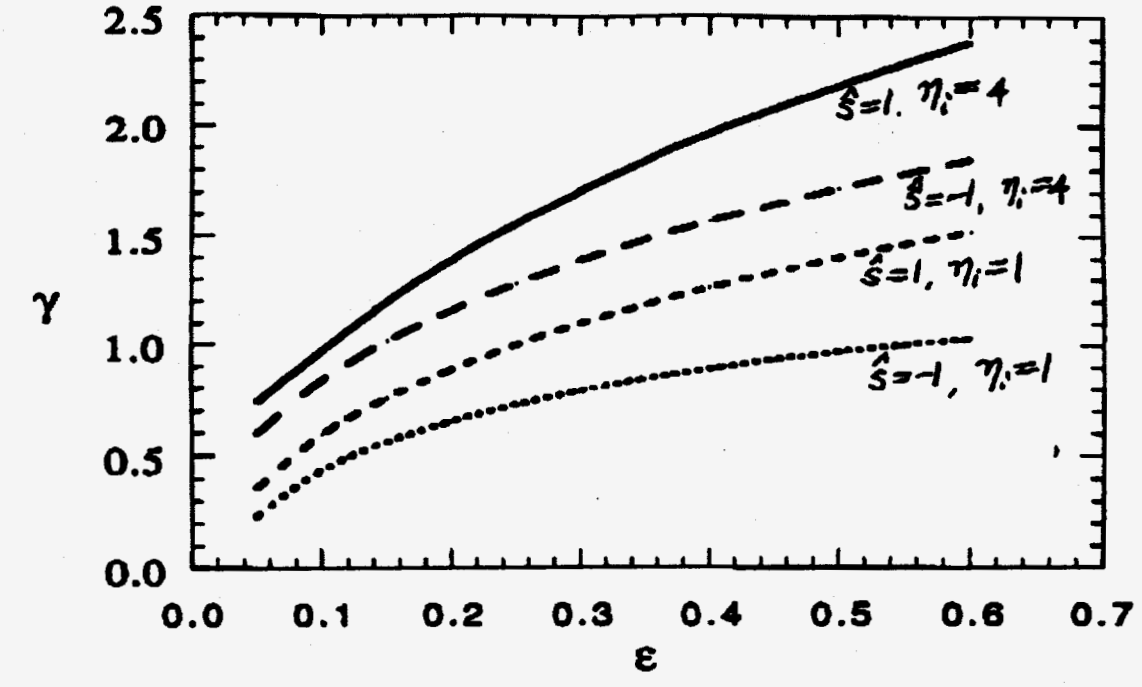
2.5
2.0
1.5
1.0
0.5
0.0
γ
0.0
0.1
0.2
0.3
0.4
0.5
0.6
0.7
ε
$\hat{s}$=1, η_i=4
$\hat{s}$=-1, η_i=4
$\hat{s}$=1, η_i=1
$\hat{s}$=-1, η_i=1

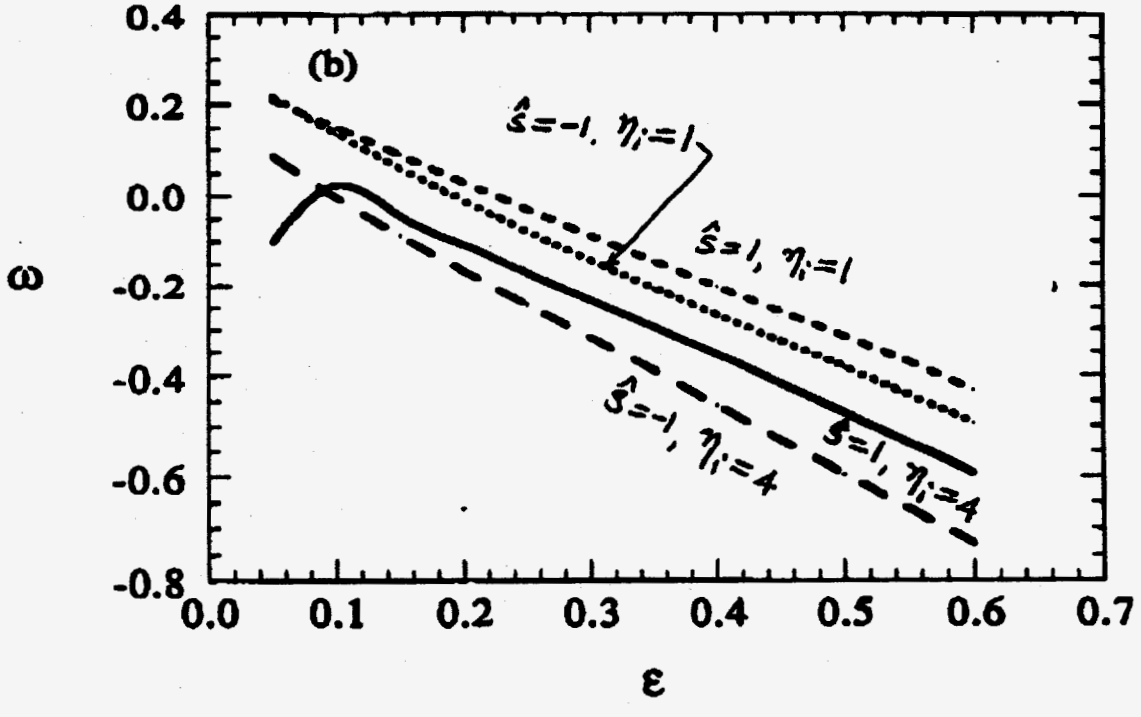
(b)
0.4
0.2
0.0
-0.2
-0.4
-0.6
-0.8
ω
0.0
0.1
0.2
0.3
0.4
0.5
0.6
0.7
ε
$\hat{s}$=-1, η_i=1
$\hat{s}$=1, η_i=1
$\hat{s}$=-1, η_i=4
$\hat{s}$=1, η_i=4

Fig.4

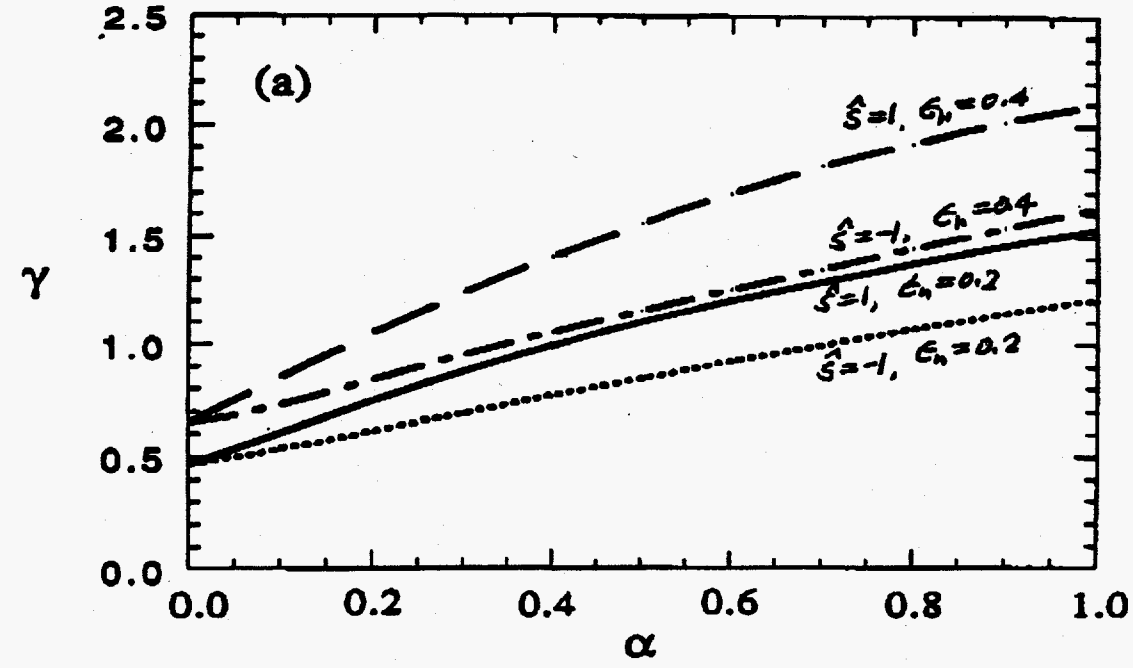
(a)
$\hat{s}=1,\ \epsilon_n=0.4$
$\hat{s}=-1,\ \epsilon_n=0.4$
$\hat{s}=1,\ \epsilon_n=0.2$
$\hat{s}=-1,\ \epsilon_n=0.2$
γ
α
2.5
2.0
1.5
1.0
0.5
0.0
0.0
0.2
0.4
0.6
0.8
1.0

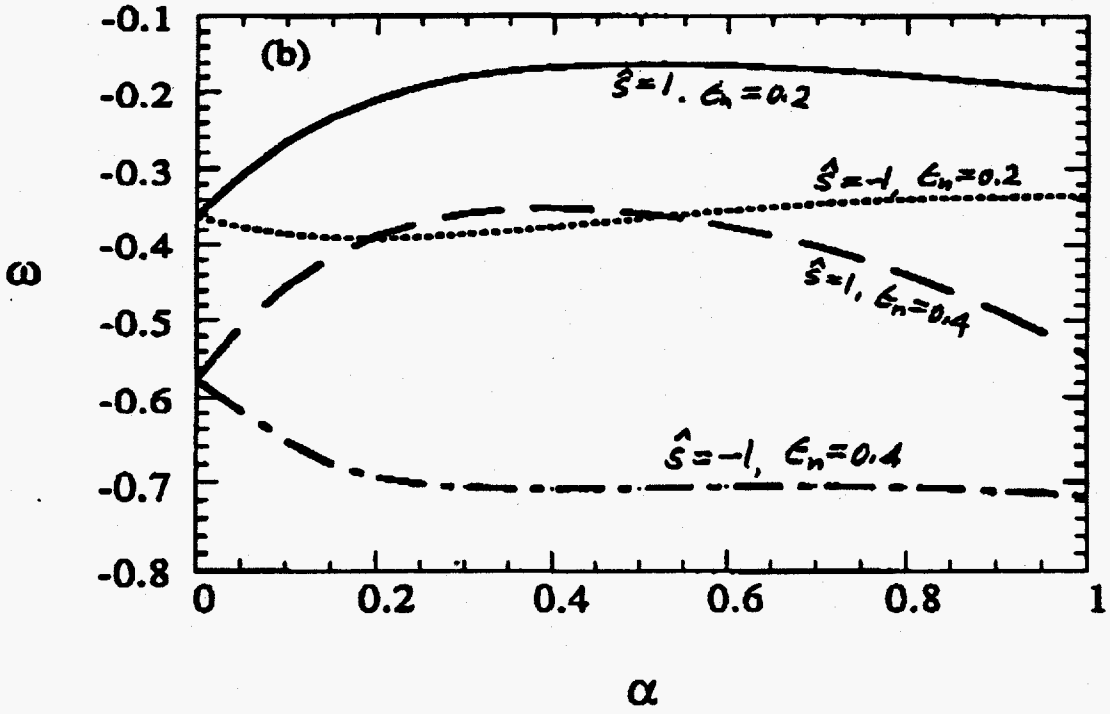
(b)
$\hat{s}=1,\ \epsilon_n=0.2$
$\hat{s}=-1,\ \epsilon_n=0.2$
$\hat{s}=1,\ \epsilon_n=0.4$
$\hat{s}=-1,\ \epsilon_n=0.4$
ω
α
-0.1
-0.2
-0.3
-0.4
-0.5
-0.6
-0.7
-0.8
0
0.2
0.4
0.6
0.8
1

Fig.5

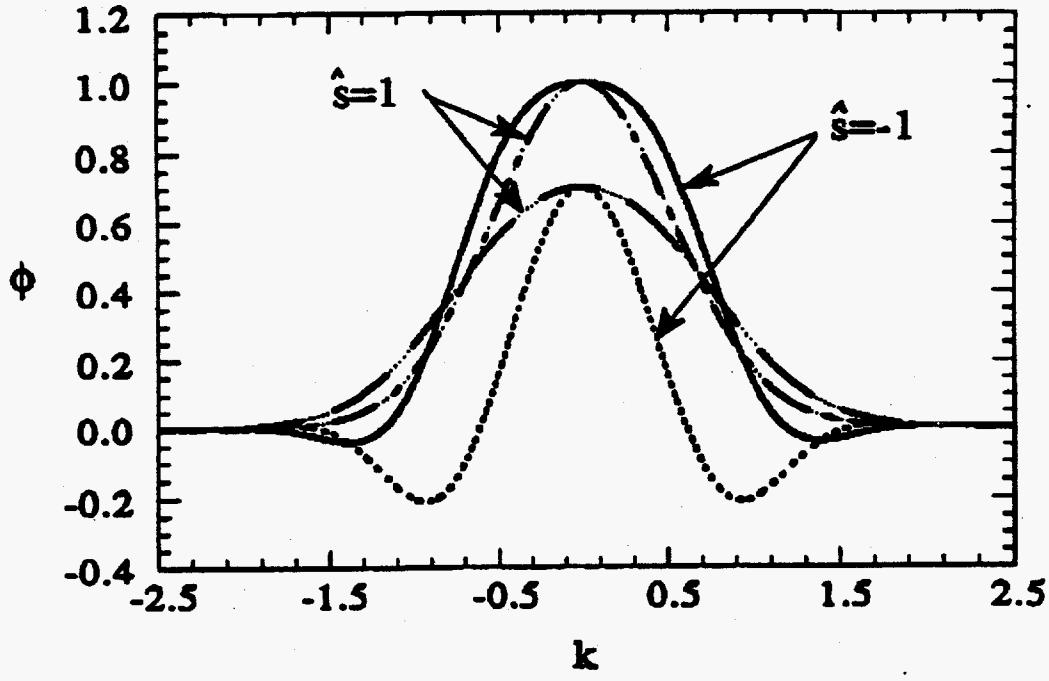

Fig.6

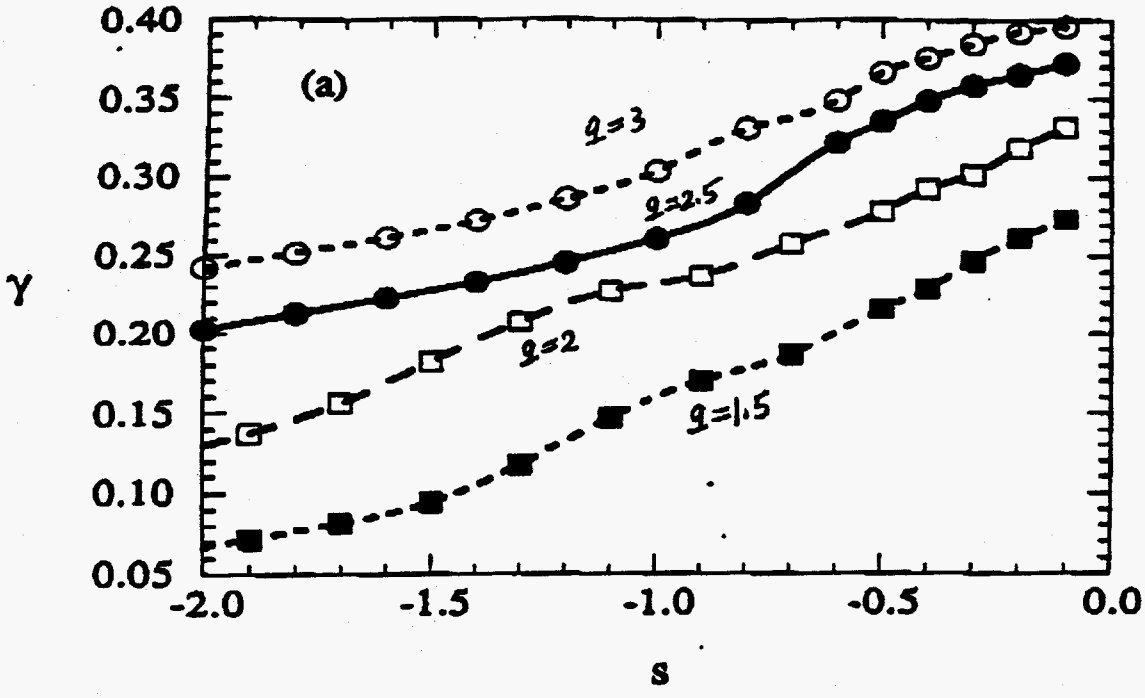
(a)
q=3
q=2.5
q=2
q=1.5
γ
0.40
0.35
0.30
0.25
0.20
0.15
0.10
0.05
-2.0
-1.5
-1.0
-0.5
0.0
s

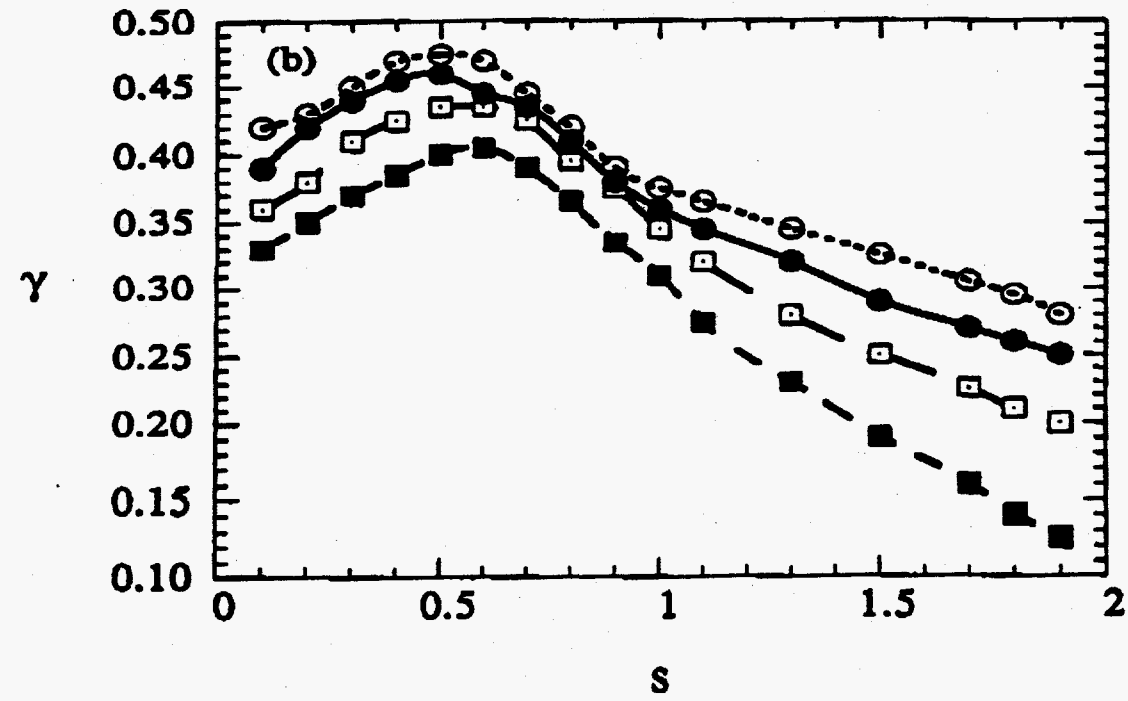
(b)
γ
0.50
0.45
0.40
0.35
0.30
0.25
0.20
0.15
0.10
0
0.5
1
1.5
2
s

Fig.7

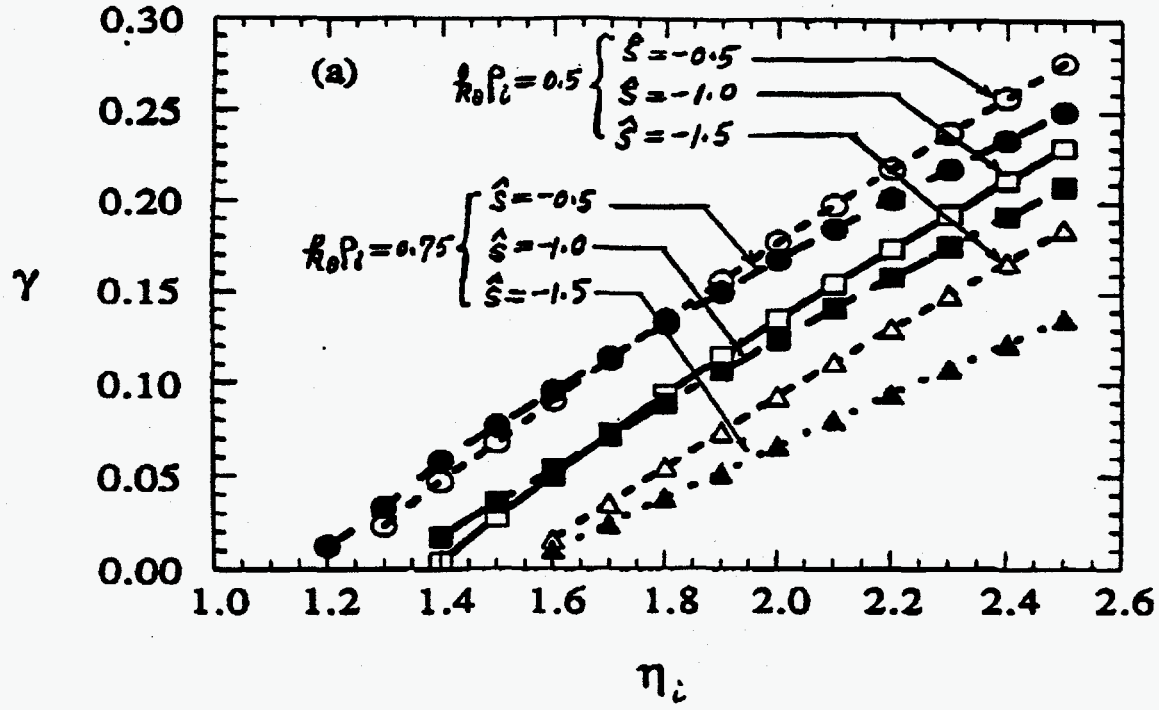
(a)
$k_0\rho_i = 0.5$
$\hat{s} = -0.5$
$\hat{s} = -1.0$
$\hat{s} = -1.5$
$k_0\rho_i = 0.75$
$\hat{s} = -0.5$
$\hat{s} = -1.0$
$\hat{s} = -1.5$
γ
0.30
0.25
0.20
0.15
0.10
0.05
0.00
1.0 1.2 1.4 1.6 1.8 2.0 2.2 2.4 2.6
η_i

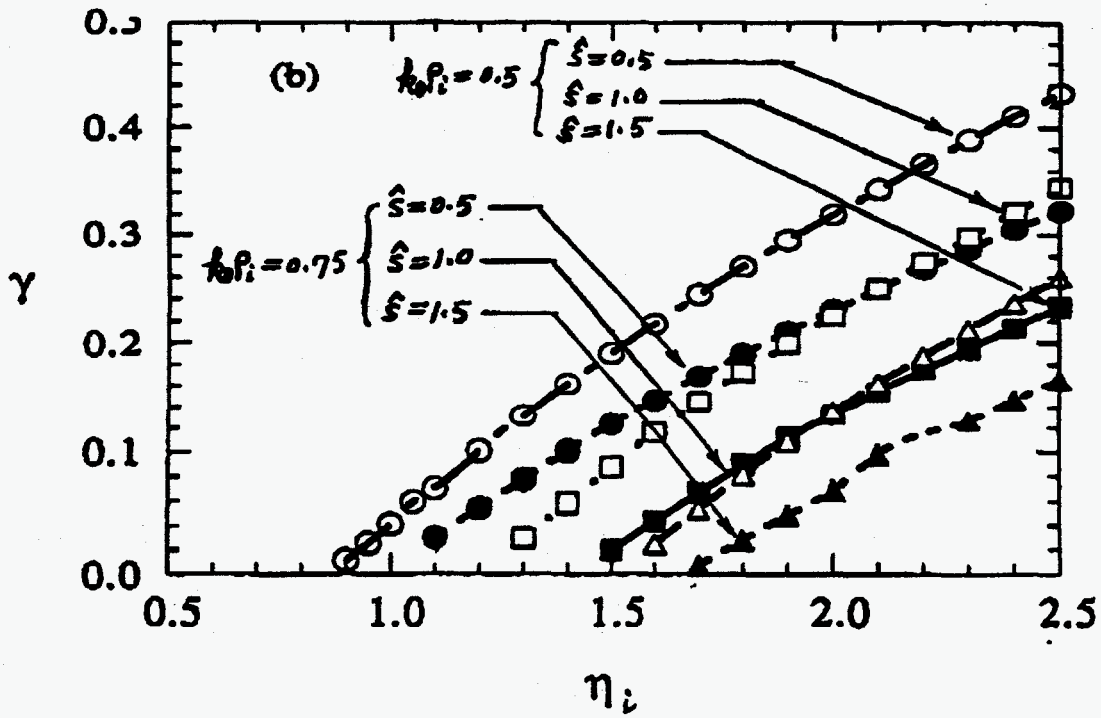
(b)
$k_0\rho_i = 0.5$
$\hat{s} = 0.5$
$\hat{s} = 1.0$
$\hat{s} = 1.5$
$k_0\rho_i = 0.75$
$\hat{s} = 0.5$
$\hat{s} = 1.0$
$\hat{s} = 1.5$
γ
0.4
0.3
0.2
0.1
0.0
0.5 1.0 1.5 2.0 2.5
η_i

Fig.8

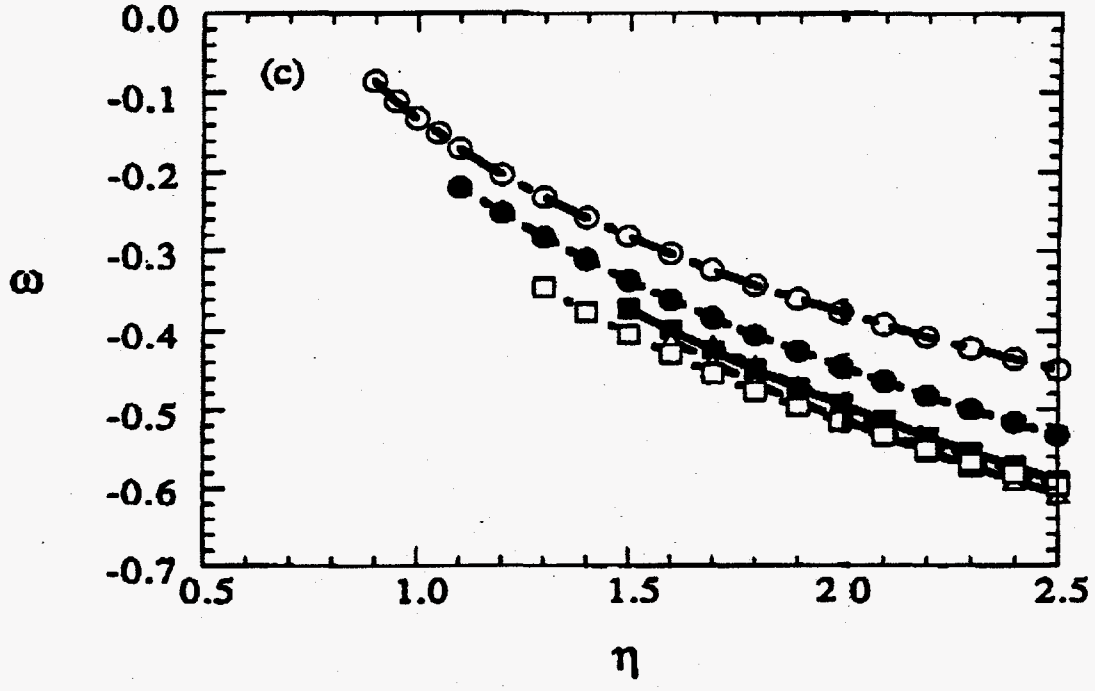

Fig.8(c)

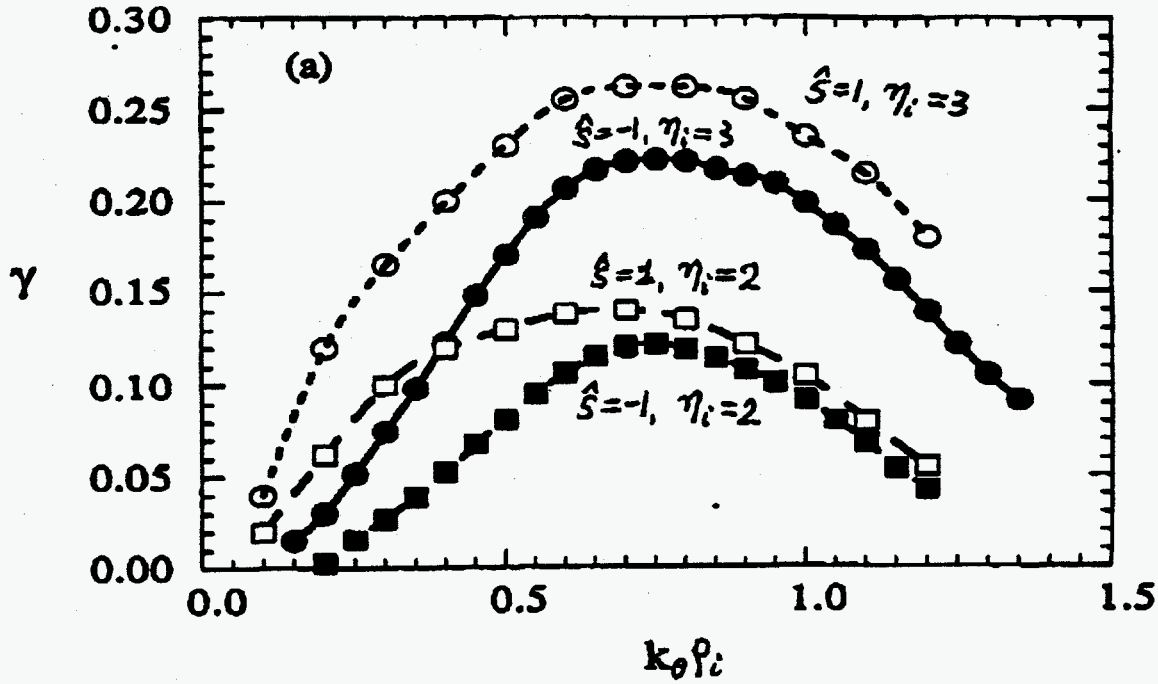
(a)
$\hat{s}=1,\ \eta_i=3$
$\hat{s}=-1,\ \eta_i=3$
$\hat{s}=1,\ \eta_i=2$
$\hat{s}=-1,\ \eta_i=2$
γ
0.30
0.25
0.20
0.15
0.10
0.05
0.00
0.0
0.5
1.0
1.5
$k_\theta \rho_i$

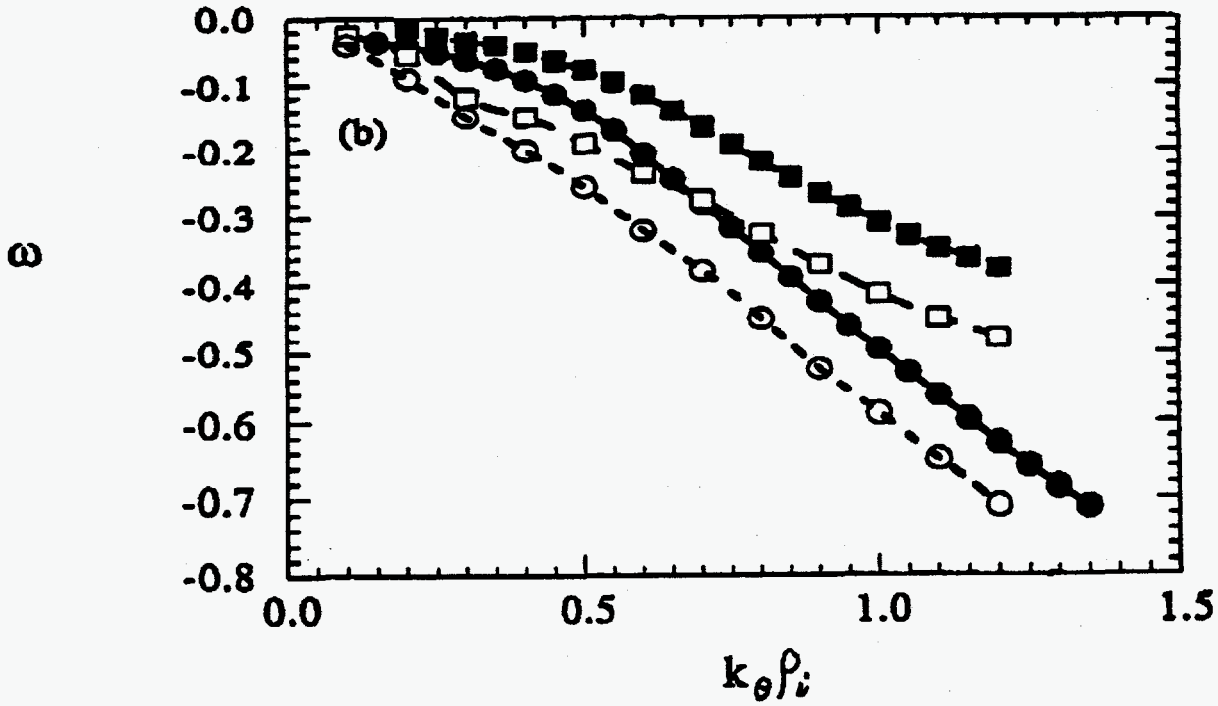
(b)
ω
0.0
-0.1
-0.2
-0.3
-0.4
-0.5
-0.6
-0.7
-0.8
0.0
0.5
1.0
1.5
$k_\theta \rho_i$

Fig.9

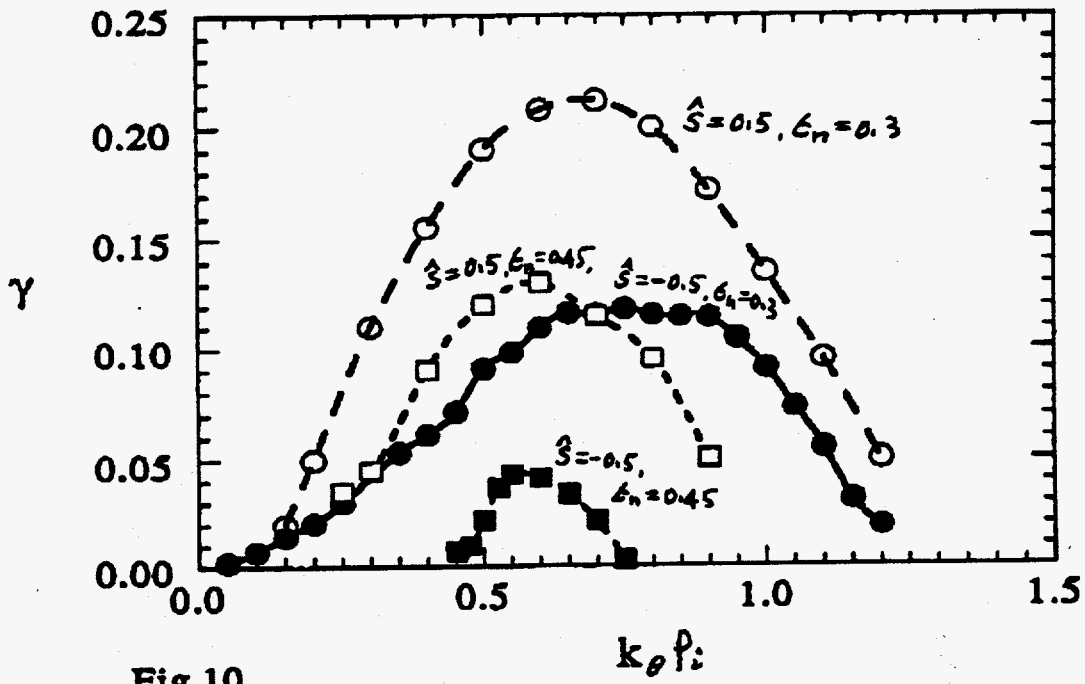
0.25
0.20
0.15
0.10
0.05
0.00
γ
0.0
0.5
1.0
1.5
$k_\theta \rho_i$
$\hat{s}=0.15, \epsilon_n=0.3$
$\hat{s}=0.15, \epsilon_n=0.45$
$\hat{s}=-0.5, \epsilon_n=0.3$
$\hat{s}=-0.5, \epsilon_n=0.45$

Fig.10

INSTITUTE FOR FUSION STUDIES
THE UNIVERSITY OF TEXAS AT AUSTIN
RLM 11.218
AUSTIN, TEXAS 78712-1060
U.S.A.